Improved CFAR Detector for Doppler-spread targets with Performance Evaluation Using Experimental Radar Dataset

Master Thesis Report

Jiaxuan Xiao

IMPROVED CFAR DETECTOR FOR DOPPLER-SPREAD TARGETS WITH PERFORMANCE EVALUATION USING REAL RADAR DATASET

MASTER THESIS REPORT

Thesis

to obtain the degree of Master of Science
in Electrical Engineering
at Delft University of Technology
to be defenced publicly on 29.08.2023

by

Jiaxuan XIAO

Born in Sichuan Province, China.

This thesis has been approved by
Responsible Professor: Dr. F. Fioranelli
Daily Supervisor: MSc Simin Zhu

Thesis committee:
Dr. F. Fioranelli, EWI-ME-MS3, Delft University of Technology
Dr. S.M. Alavi, EWI-ME-ELCA, Delft University of Technology
MSc Simin Zhu, EWI-ME-MS3, Delft University of Technology

ACKNOWLEDGEMENTS

First, I want to express my deepest gratitude to my supervisors Dr. Francesco Fioranelli and Simin Zhu. Without their help and support, I could not have completed this thesis. They not only provided professional suggestions to guide me in exploring the topics but also supported me when I felt anxious and stressed. I am profoundly grateful for their constant patience and support. They are always ready to provide me with invaluable guidance and assistance.

I would like to thank all members of Microwave Sensing, Signals and Systems (MS3) Group and friends for their continuous encouragement and discussions.

Additionally, I am thankful to my family for their love and support. This achievement would not have been possible without their understanding and support.

At last, my master program at TU Delft has come to an end. I am looking forward to the next steps. All the best to everyone I love and who helps me!

ABSTRACT

Autonomous driving can bring revolutionary advancements in transportation, by making vehicles navigate and operate independently without human intervention. To achieve this, autonomous vehicles are equipped with sensors, including cameras, Light Detection and Ranging (LiDAR), and radar, which provide them with a comprehensive view of their surroundings. Frequency-Modulated Continuous Wave (FMCW) radar is the most popular radar sensor employed on autonomous vehicles (AVs), for its long working distance, simultaneous accurate measurements of range and radial velocity of the target, and its robustness for all weather conditions. However, there are still many problems to be solved for FMCW radar for detecting vulnerable road users (VRUs), such as pedestrians. The Constant False Alarm Rate (CFAR) detector plays a crucial role in FMCW radar signal processing, for its adaptive capability to estimate multiple potential targets versus variable clutter and noise backgrounds, and it is often the first step of processing in many automotive radar pipelines.

There have been several published methods for detecting pedestrians. However, most methods hardly consider public real-world radar datasets for their performance evaluation. Meanwhile, conventional CFAR used in autonomous driving, such as Cell averaging CFAR (CA-CFAR) and Ordered-statistic CFAR (OS-CFAR) are not specially designed for Doppler-spread targets (DSTs), while pedestrians are typical DSTs which shows Doppler extension in range-Doppler-map (RDM). This is due to the movement of the arms and legs of pedestrians that make them not only extended targets at mm-wave frequencies but also present a spread Doppler signature.

Therefore, in this thesis a proposed CFAR detector for DSTs enhances the probability of detection compared to two-dimensional (2D) CA-CFAR and two-dimensional (2D) OS-CFAR. The parametric study is conducted on CA-CFAR and OS-CFAR detectors. Additionally, the computation time is reduced dramatically.

CONTENTS

LIST OF TABLES

List of Figures

List of Abbreviations

1D one-dimensional. 17, 20–22, 24, 27, 29, 30, 32

2D two-dimensional. vi, x, xi, 4, 6, 10, 15, 17–20, 22, 24, 27–30, 32

ADC analog-to-digital. x, 4

AVs autonomous vehicles. vi, ix, 1–3, 8, 13, 31

CA-CFAR Cell averaging CFAR. vi, ix–xi, 4, 6, 12, 13, 17, 18, 22, 24–32

CDF cumulative distribution function. 36

CFAR Constant False Alarm Rate. vi, ix–xi, 3–8, 12–14, 17, 21, 22, 27–32

CUT cell under test. x, xi, 12, 18, 19

CW Continuous Wave. 8

DBSCAN Density-based spatial clustering of applications with noise. 3

DSTs Doppler-spread targets. vi, 5–7, 14, 17, 20–22, 27, 28, 30, 31

FFT fast Fourier transform. x, 4, 9, 10, 17

FMCW Frequency-Modulated Continuous Wave. vi, x, 1, 3, 4, 6, 8, 9, 13, 31

GO-CFAR greatest-of-CFAR. x, 12, 13

LiDAR Light Detection and Ranging. vi, 1, 3

MIMO Multiple Input Multiple Output. 14

MMW Millimeter-Wave. 1

OS-CFAR Ordered-statistic CFAR. vi, ix–xi, 4–6, 12, 13, 19–22, 24–32

PDF probability density function. xi, 11, 36

RCS radar cross Section. 6–8, 20, 28, 30

RDM range-Doppler-map. vi, x, xi, 4, 10, 12, 16–20, 22, 24, 27–29, 32

ROC Receiver Operating Characteristic. xi, 23, 24, 26, 27, 29–32

Rx receiver antennas. 14

SNR signal-to-noise ratio. 6, 7

SO-CFAR smallest-of-CFAR. x, 12, 13

Tx transmitter antennas. 14

UKF Unscented Kalman Filter. 3

VRUs vulnerable road users. vi, 1, 7, 20, 31

1

INTRODUCTION

1.1. AUTONOMOUS DRIVING

The potential of autonomous vehicles (AVs) as an alternative mode of transportation has drawn significant attention from both within and outside industry [1], [2]. This section examines the impact of AVs on traffic safety and congestion, considering their advanced sensor technologies and potential to reduce human error:

1. **AVs can reduce accidents and losses through advanced sensors.** The widespread adoption of AVs will significantly impact everyone's current way of life. The equipped onboard sensors in vehicles have the potential to help reduce traffic accidents and financial loss because they improve the human perception of the environment and minimize human error. In general, Millimeter-Wave (MMW) FMCW radar, camera, LiDAR are primarily used for their fast senses of everything on the road. AVs integrate video cameras that are installed from different viewpoints, AVs are offered 360° observation of their external surroundings. FMCW radar sensors transmit signals and measure the distance, velocity, and azimuth of objects in relation to the vehicle in real time. LiDAR works similarly with radar, albeit employing lasers rather than radio waves. LiDAR can create three-dimensional visual representations of detected items and the comprehensive mapping of the surroundings.

2. **AVs can reduce human errors.** The U.S. Department of Transportation estimates that there was a total of approximately 7,277,000 police-reported traffic accidents in 2016, accounting for 37,461 fatalities and approximately 3,144,000 injuries [3]. Over half of all fatalities worldwide are caused by VRUs, including motorcyclists, cyclists, and pedestrians, and 26% of fatalities involve pedestrians and cyclists according to World Health Organization [4]. Human errors are to blame for 94% of motor vehicle collisions [5]. It is discovered that other human errors, such as distraction or speeding, regularly cause car crashes, suggesting the scope of potential human error even when the vehicle, roadway, or environment is the primary reason for the crash. Therefore, the popularity of AVs can contribute to alleviating human errors and increasing the safety of every road traffic participant.

3. **AVs can help address traffic safety and congestion challenges.** Simulations predicted that replacing all light vehicles on French roads with AVs will reduce injury crashes and fatal crashes by about 60% [6]. Additionally, the flow will be smoothed out and bottlenecks will be reduced, which will relieve the traffic congestion. The predicted reduction in highway congestion delays for all cars is 15% at the level of 10% AV market penetration. This analysis projects a 35% reduction in freeway delays at the 50% market penetration level. Lastly, it is assumed that freeway congestion will decrease by 60% at the 90% level [7].

The six progressive levels of autonomy for self-driving cars are described on a scale (from 0 to 5) by the Society of Automotive Engineers International [8]. Table 1.1 illustrates the spectrum of autonomy, encompassing six levels that progress from "No driving autonomy" (Level 0) to "Full driving autonomy" (Level 5).

Level	Name	Description
0	No driving autonomy	The responsibility for the driving encounter lies entirely with the driver.
1	Driver assistance	Vehicle systems are integrated to provide support. Meanwhile, drivers remain actively engaged.
2	Partial driving autonomy	Although the system can manage steering, acceleration, and braking, at level 2, the driver's participation and consciousness are still required.
3	Conditional driving autonomy	While the driving system handles all driving functions comprehensively, it's essential for the driver to be prepared to assume control when required.
4	High driving autonomy	When malfunctions occur, vehicles can take action without the need for immediate driver participation. Nevertheless, the driver is able to manually assume control of the vehicle.
5	Full driving autonomy	Regardless of driving conditions or road state, driving systems require no human involvement.

Table 1.1: The six levels of driving autonomy [8]. The levels progress from no autonomy, through partial driving autonomy, conditional driving autonomy, and high driving autonomy, to full driving autonomy.

There are no fully AVs on the market yet. Many vehicles today have features that help drivers in particular situations, like preventing drivers from swerving out of lane or assisting drivers in stopping in time to prevent an accident or lessen its severity. Recent vehicles are equipped with hardware like cameras and radar, to prevent drifting into other lanes, make risky lane changes, or warn other drivers when they are backing up their cars. These Level 1 AV driver assistance technologies have proliferated in automobiles

in recent years. Based on National Highway Traffic Safety Administration's analysis, it is predicted that more fully automated safety features will be implemented in AVs through 2025 [9].

Therefore, regardless of the type of sensor, it is crucial to enhance their detection accuracy and efficiency by applying more advanced algorithms, which is essential for achieving full driving autonomy.

1.2. SENSOR COMPARISON AND RADAR PROCESSING PIPELINE

The sensors that have been installed heavily influence the quality of information that AVs will receive. Table 1.2 provides an overview of the pros and cons of the aforementioned sensors.

Sensor	Advantages	Disadvantages
FMCW Radar	1) Long working distance 2) Small in dimension 3) Robust for all-weather	1) Poor detection of relatively stationary objects 2) Poor azimuth and elevation resolution
Camera	1) Providing a colorful perspective of the environment 2) Small in dimension	1) Powerful computation system required 2) Sensitive to heavy rain, fog and snowfall
LiDAR	1) High angle resolution 2) Wide field of view	1) High cost 2) Highly influenced by adverse weather

Table 1.2: The list of pros and cons of sensors on AVs [10]

In conclusion, while cameras, LiDAR, and FMCW radar each have their strengths and limitations, the abilities of FMCW radar that provides accurate range and velocity information of objects in relation to the radar in real time, sets it apart as an essential tool for enhancing the capabilities of AVs. Also, FMCW radars detect at long distances and are more robust under lighting or adverse weather conditions than cameras and LiDAR. FMCW radars are relatively cheap and compact making it practical to employ multiple units, thereby enhancing overall performance [11].

CFAR detector is a critical component in FMCW radar signal processing shown in Figure 1.1, specifically tailored to enhance the detection capability of FMCW radar systems. The CFAR algorithm assesses the statistical properties of the received signal of a potential target echo and calculates the detection threshold adaptively. This adaptive threshold allows the radar system to detect valid target echoes against background noises, clutter, and interferences, thus enhancing the accuracy and reliability of target detection. Therefore, CFAR is an important step in FMCW radar processing. The target echoes after CFAR are initial steps preceding a series of critical operations. Clustering involves the application of algorithms like Density-based spatial clustering of applications with noise (DBSCAN) to group relevant targets. Tracking employs methods such as the Unscented Kalman Filter (UKF) to trace target trajectories over time. Classification and

segmentation are carried out using techniques like Neural Networks, distinguishing various target types and marking out distinct regions within the environment respectively. This sequence of processes contributes to the comprehensive analysis of FMCW radar data.

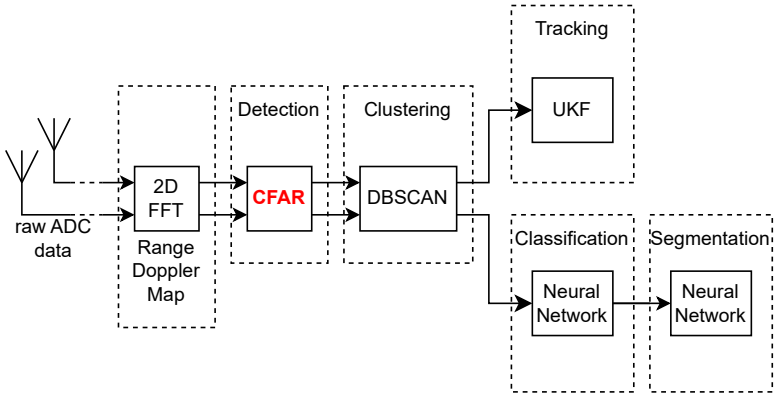

Figure 1.1: Conventional FMCW radar signal processing pipeline. The FMCW radar data processing encompasses the stages of raw analog-to-digital (ADC) data, RDM generated by 2D fast Fourier transform (FFT), and the subsequent application of clustering, tracking, classification, and segmentation for target analysis. The detection stage via CFAR algorithm is highlighted as the block this thesis focused on.

1.3. CONTRIBUTIONS OF THIS THESIS

The primary contribution of this thesis is summarized as:

- Use a public real-world radar dataset to compare three CFAR detectors in the same scenario. This usage of experimental data guarantees practical environmental information that is difficult to replicate in simulated software to evaluate and enhance the robustness of radar detectors.
- Propose a modified CFAR detector that detects both the range and the Doppler information of targets exhibiting a spread signature in Doppler, which is typical of pedestrians and cyclists in automotive radar. This detector improves the probability of detection under the same probability of false alarms compared to 2D CA-CFAR and 2D OS-CFAR. Meanwhile, the proposed method decreases the computation time by reducing the search dimension in RDM.

1.4. THESIS OUTLINE

In chapter 2, the challenges caused by pedestrians and related work about detecting pedestrians with automotive radar are reviewed. The research questions are also included. The principles of FMCW radar and the detection fundamentals are provided in chapter 3. In addition, the chapter covers the principles of CFAR techniques, highlighting their significance in radar target detection. The focus of chapter 4 is on the

description of the utilized real-world radar dataset and its properties. Then, this chapter introduces three conventional CFAR algorithms, explaining their working principles. Furthermore, the chapter presents the proposed modified OS-CFAR tailored to DSTs that detects both range and Doppler information of targets. Chapter 5 presents the outcomes of the study's experiments, including the analysis of ROC curves. The parametric study of two CFAR detectors and their performance among three kinds of targets. Additionally, computational costs associated with each algorithm under different parameter settings among targets are discussed. Chapter 6 concludes the research findings and the contributions of the study. Meanwhile, some potential avenues for future research and improvements are provided.

2

Literature Review

This chapter touches on the intricate landscape of radar target detection, focusing on the particular solutions to the challenges caused by Doppler-spread targets (DSTs). The targets with their extension in the Doppler spectrum, resulting from the micromotion of pedestrian limbs when walking, are called DSTs. These challenges emerge from the low signal-to-noise ratio (SNR) and dispersed received energy because of DSTs. Solving these challenges demands robust detection methods that can detect weak target echoes amid clutter and noise. In addressing these challenges, researchers have extensively explored the application of various CFAR detectors.

2.1. Related Work

There have been several published methods for detecting pedestrians with autonomous radar. The primary approach to address the challenges associated with pedestrians of small RCS is to enhance the qualities of the reflected echoes and mitigate the impact of clutter. Clutter refers to unwanted echoes that appear in a radar system's received signal due to various non-target sources, such as reflections from the ground, buildings, and other objects in the environment. The masking effect caused by other targets can be mitigated by 2D CFAR [12], but algorithms with this family are typically designed for point targets. Conventional CFAR detection methods for point-based targets, such as CA-CFAR and OS-CFAR [13], fail to utilize the Doppler-spread information from pedestrians. They will perform worse because of the low SNR and dispersed received energy [13]; this is particularly true in the case of automotive radar where the wide bandwidth and the short wavelength with respect to the target size makes the point target assumption not valid. In [14], by utilizing the diagram features in the range-Doppler domain with 77-GHz FMCW radar, a deep recurrent neural network-based pedestrian detection approach was presented. However, maintaining a high detection performance requires a longer period for collecting data, which is not always operationally possible in automotive scenarios. A waveform based on the interlaced chirp sequence was developed to improve range and Doppler resolution, leading to the improved detection performance

of pedestrians [15]. By using a coherent phase difference method, the information about pedestrians is separated from the background noise [16]. Zhang et al. proposed the target energy accumulation along continuous Doppler cells to improve the ability to detect [17], but this approach fails to detect the Doppler velocity of targets. Despite the aforementioned approaches, to the best of the author's knowledge the detection of pedestrians and DSTs in automotive radar is still a challenge.

2.2. PRESENT GAPS

Pedestrians are the most important class of VRUs on the urban road. FMCW radar still faces difficulty in reliably detecting pedestrians. The radar cross Section (RCS) of a pedestrian is about −8 dBsm [18], causing weak reflected energy. Therefore, when pedestrians are walking on the road, they are easily hidden by other strong reflections, such as buildings and trucks [19]. As a result, the facts above will degrade the detection performance of pedestrians, which leads to worse performance of subsequent tracking and classification, as shown in Figure 1.1. It is important to note that conventional CFAR detectors are not optimized for the challenges of DSTs.

In addition, although recent related work has made great progress, most of them have not considered the actual road traffic scenarios or just use their own created (oftentimes simulated) scenarios, rather than a publicly available dataset. These created scenarios are impractical to duplicate to obtain the same environmental noise, clutter, etc. Therefore, assessing detectors using public real-road traffic datasets is crucial. Firstly, it allows for a realistic understanding of how these detectors perform in complex and dynamic traffic scenarios. Real datasets encompass diverse environmental conditions and vehicle behaviors that may not be fully captured in simulated environments. Secondly, evaluating CFARs with actual road traffic data helps identify potential challenges and limitations that might arise during real-world deployment. This process aids in refining the algorithms to enhance their robustness and reliability. Also, using a public dataset contributes to the comparisons of other radar detectors in the same scenario. Overall, assessing CFAR detectors in real road traffic datasets ensures that these algorithms are well-equipped to handle the complexities of driving scenarios, ultimately facilitating safer and more efficient autonomous driving systems.

2.3. SUMMARY

Enhancing the detection quality of DSTs, especially pedestrians, in automotive radar is important. Otherwise, poor detection results will jeopardize following radar perception, such as clustering, tracking, classification, or segmentation shown in Figure 1.1. Meanwhile, the small size of pedestrians results in them being masked by stronger radar reflections and DSTs lead to the low SNR because of the dispersed energy in the Doppler spectrum. Some advanced CFAR detectors are proposed to address such problems and enhance the target detection capability but are not evaluated on a public real-world radar dataset, which can be compared with other widely used radar detectors in the same scenario. Therefore, some more work is needed to be done around these problems.

3

FUNDAMENTALS OF FMCW RADAR AND TARGET DETECTION

In this chapter, a foundational guide of FMCW radar is presented in section 3.1 including the formulas of the transmitted and received signal, and the critical parameters determining range and velocity resolution. Section 3.2 is around the core concept of target detection and delves into the fundamentals of target detection in radar. A comprehensive exploration of the CFAR family of algorithms is presented, emphasizing its significance in the adaptive estimation of clutter power and scaling factor in section 3.3.

3.1. FMCW RADAR

The radar equation is a fundamental formula in radar systems that relates the transmission power P_t, transmit antenna gain G_t, receive antenna gain G_r, wavelength λ, RCS of the target σ and the distance between the radar and the target d and the received power P_r, given in (3.1). It tells factors that influence the strength of the received radar signal and helps to understand how the performance of a radar system can be optimized.

$$P_r = \frac{P_t \cdot G_t \cdot G_r \cdot \lambda^2 \cdot \sigma}{(4\pi)^3 \cdot d^4} \tag{3.1}$$

Due to their robustness in all-weather conditions and their ability to measure radial velocity by modulating a carrier wave with a high frequency over a specific bandwidth, FMCW Radars have commonly deployed on AVs. Continuous Wave (CW) radar emits continuous electromagnetic waves. One key advantage of CW radar is its capability to determine target velocity through the Doppler effect, attained by measuring the frequency shift between transmitted and received signals. However, CW radar lacks the ability to estimate range due to its absence of frequency modulation. In contrast, FMCW radar exploits frequency changes between transmitted and received signals during modulation, facilitating accurate range estimation. FMCW radar that provides accurate range and velocity information between radar and targets. The FMCW radar transmits a sequence of chirp signals. A "chirp" refers to a continuous and linearly varying frequency

signal that is emitted by the radar transmitter. The term "chirp" is used because the frequency of the signal increases or decreases in a manner that resembles the sound of a bird chirping. Figure 3.1 illustrates how the measurement is carried out by using a sawtooth modulation pattern. The Doppler shift effect causes an upward displacement. As a consequence of the time delay, the received signal (red dashed line) moves to the right.

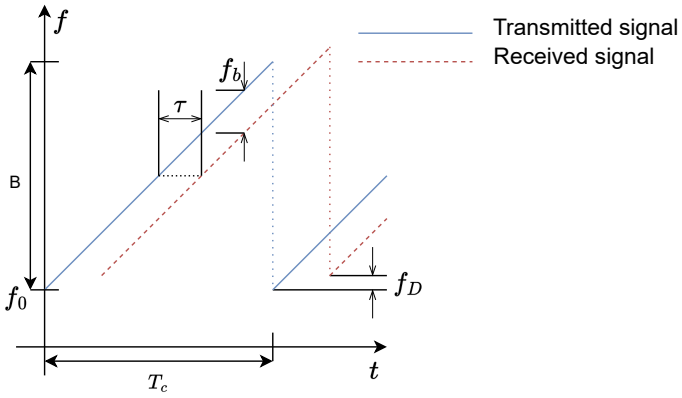

Figure 3.1: Range and velocity measurement of the FMCW radar with the sawtooth shape modulation. The time it takes for the transmitted signal to travel to the object and return as the reflected signal is measured. Since the speed of electromagnetic waves is constant (the speed of light), the time delay can be directly converted into a distance measurement.

where τ is the time delay between the transmitted and received signals in seconds and f_D is Doppler frequency caused by the relative move to the radar. B is the bandwidth of the signal, T_c is the time of each chirp, f_b is the beat frequency due to a frequency difference between the transmitted signal frequency and the reflected signal frequency and f_0 is the carrier frequency.

In FMCW radar hardware, a mixer stage combines the transmitted signal and received signal and outputs beat frequency f_b, illustrated in Figure 3.1. The first FFT is applied to the beat signal and converts it from the time domain to the frequency domain. The distance of the target in relation to the radar is given by (3.2),

$$d = \frac{f_b c}{2k} \tag{3.2}$$

where $k = B/T_c$ is the chirp rate, illustrated in Figure 3.1.

The range resolution d_{res}, also known as the smallest distance that can be measured between two objects, is given as (3.3),

$$d_{res} = \frac{c}{2B} \tag{3.3}$$

The measured velocity (3.4) is determined by Doppler frequency f_D. The maximum relative velocity that the radar measures and there is a limit to the smallest velocity dif-

ference that the radar can measure between two moving targets, determined by (3.5) and (3.6) respectively,

$$v = \frac{\lambda f_D}{2} \quad (3.4) \qquad v_{max} = \frac{\lambda}{4T_c} \quad (3.5) \qquad v_{res} = \frac{\lambda}{2T} \quad (3.6)$$

with v_{res} the velocity resolution and T the observation time.

Figure 3.2 shows the Range-Doppler processing strategy. The received signal is sampled and each chirp signal (also called fast time) is treated individually by FFT. Then, the received signal is divided into several range bins. In a subsequent stage, the second FFT is applied within each range bin (also called slow time) to determine the Doppler frequency f_D of a radar target. In this instance, rows of 2D matrix are individually subjected to FFT, resulting in RDM, which provides a great capability to resolve the interested target with different relative velocities and ranges [12].

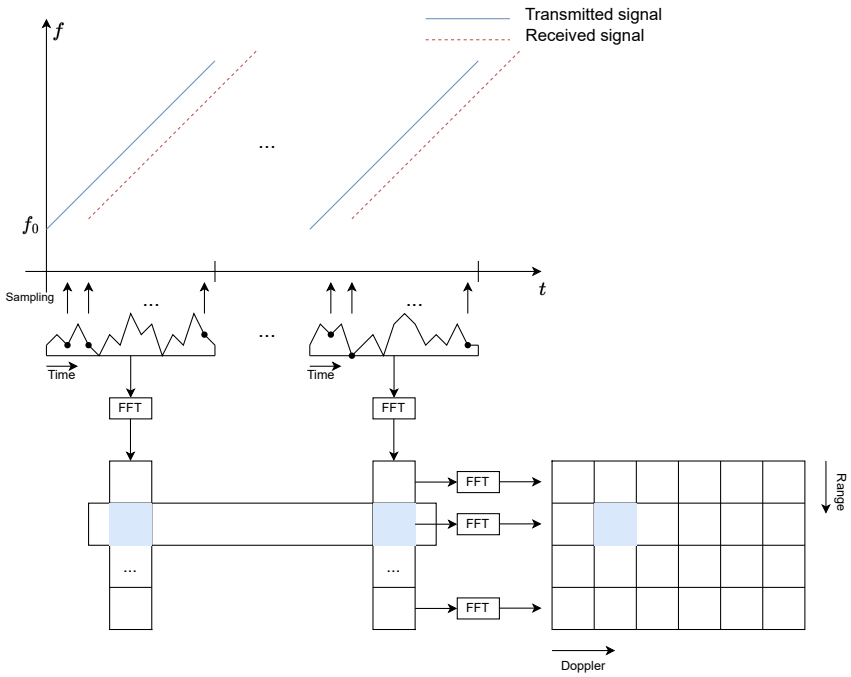

Figure 3.2: Range-Doppler processing strategy [12]. The first FFT is applied to each chirp signal. Subsequent to this, the acquired signal is divided into multiple range bins. Then, a second FFT analysis is implemented within each range bin to extract the Doppler frequency f_D associated with a radar target. The output signal is RDM.

3.2. DETECTION FUNDAMENTALS

Hypothesis testing is a statistical method to make inferences about parameters based on the analysis of experience data. There are two types of hypothesis testing as below [20]:

- **Null Hypothesis:** In hypothesis testing, the null hypothesis is the default model as a starting point for the analysis, denoted as H_0. It is a statement of no relationship between variables in a statistical hypothesis test.
- **Alternative Hypothesis:** It is the complementary statement to the null hypothesis in hypothesis testing, proposing a specific relationship between variables in the experiment data, denoted by H_1.

p_{fa}, called the probability of false alarm, refers to the probability of incorrectly rejecting H_0 when a test chooses H_1. The detection performance of a detector can be measured by p_{fa} (3.7),

$$p_{fa} = p(H_1; H_0) = p(Y_0 \geq T \cdot Z) = \int_S^{\infty} f_{Y_0}(y) \tag{3.7}$$

where T is the scaling factor, S is the detection threshold, and the estimated clutter power is denoted as Z. $f_{Y_0}(y)$ is the probability density function (PDF) of the clutter.

Neyman-Pearson Lemma provides a theoretical framework to determine the decision rule that maximizes the probability of detecting while keeping the probability of false alarm at a fixed level [21], demonstrated in Figure 3.3. A decrease in the probability of false alarms will result in a drop in the probability of detection.

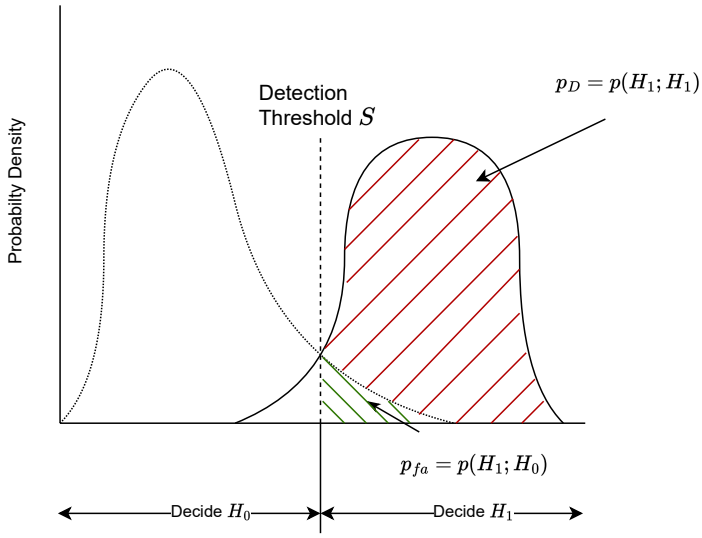

Figure 3.3: Neyman-Pearson Lemma: Hypothesis Test. It is a fundamental concept in statistical hypothesis testing, specifically in the context of binary hypothesis testing. It provides a framework for making decisions between two competing hypotheses while optimizing the trade-off between the probability of false alarm and detection.

A detection algorithm in radar systems is used to filter noise and clutter. Each target can be in a region with a different cluster level. If a fixed threshold is set, it will yield false

alarms or miss detections depending on this value. Therefore, an adaptive detection threshold algorithm is needed to provide more accurate detection results.

3.3. BASIC CFAR PRINCIPLES

In real scenarios, clutter in the environment always has an impact on targets. Targets are hidden by the noise, clutter, and interference inside the RDM and suffer from false alarms because of a wide variety of objects during driving, such as railings, road signs, and traffic cones. A frequently used detector is CFAR [22], which calculates the detection threshold adaptively and only keeps a portion of the returned signal if it is above a predetermined threshold [23]. A too-high threshold will produce low false positives and high false negatives, whereas a low threshold will cause high false positives. The fundamental operations of various basic CFAR detectors [23], [24], [25] are shown in Figure 3.4.

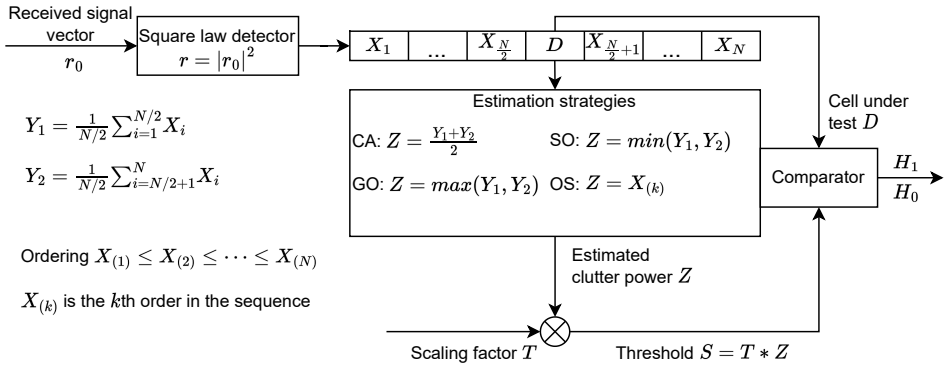

Figure 3.4: The steps of CA-CFAR [23], GO-CFAR [24], SO-CFAR [25] and OS-CFAR [23] detectors. These four conventional CFAR detectors differ from various strategies in the estimation of clutter power and scaling factor.

The square of the received signal amplitude vector $r = |r_0|^2$ is obtained by the square law detector. The center sample in the detection window is the cell under test (CUT) D. On both sides of CUT are the leading window and the lagging window with lengths of $N/2$. The clutter power Z is estimated based on the leading window and the lagging window by different estimation strategies. The mean value of the reference cells Y_1 and Y_2 surrounding CUT is determined by the leading window and the lagging window, represented by (3.8) and (3.9).

$$Y_1 = \frac{1}{N/2}\sum_{i=1}^{N/2} X_i \tag{3.8}$$

$$Y_2 = \frac{1}{N/2}\sum_{i=N/2+1}^{N} X_i \tag{3.9}$$

where X_i is the ith unit in the RDM.

For the CA-CFAR detector, the clutter power Z_{CA} is obtained by the mean value of Y_1 and Y_2 [26], shown as (3.10).

$$Z_{CA} = \frac{Y_1 + Y_2}{2} \tag{3.10}$$

When multiple targets are present within the same reference window, it leads to the masking of these targets [27].

When it comes to the GO-CFAR, the clutter power level is determined by the maximal value of Y_1 and Y_2 [24]. Instead, the noise level is obtained by the minimal value of Y_1 and Y_2 in the SO-CFAR detector [25], demonstrated in (3.11) and (3.12).

$$Z_{GO} = max\{Y_1, Y_2\} \tag{3.11}$$

$$Z_{SO} = min\{Y_1, Y_2\} \tag{3.12}$$

In the OS-CFAR, the reference cells are ordered in ascending order $X_{(1)} \leq X_{(2)} \leq ... \leq X_{(N)}$. The clutter level Z_{OS} is determined by the kth smallest reference sample [23], followed as (3.13).

$$Z_{OS} = X_{(k)} \tag{3.13}$$

The procedure for target detection is founded on a hypothesis test, where H_0 is used to hypothesize the existence of noise alone, and H_1 is used to describe a scenario involving a target combined with noise. The hypothesis is followed as (3.14),

$$d(Y) = \begin{cases} target & \text{if } Y \geq S \\ no\ target & \text{if } Y < S \end{cases} \tag{3.14}$$

where the detection threshold S is calculated as the product of scaling factor T and the estimated clutter power Z (3.15):

$$S = T \cdot Z \tag{3.15}$$

3.4. SUMMARY

In this chapter, the background information of FMCW Radar, CFAR detection algorithm and the target detection is introduced. FMCW Radar continuously emits a frequency-modulated signal to measure target distance and speed. Based on the fundamentals of target detection and CFAR, various CFAR detectors are proposed. Among these detectors, CA-CFAR and OS-CFAR are two widely used algorithms in AVs [28], which will be discussed in detail in the next chapter.

4

PROPOSED METHODOLOGY

In order to evaluate the detection performance of different detectors in a public dataset, several CFAR detectors are selected, which include conventional CFARs and some new CFARs. An in-depth exploration of the dataset's features and distribution is conducted in subsection 4.1.1 and the details of algorithms are introduced. In subsection 4.1.2, a detailed description of the dataset pre-processing procedures is provided. Furthermore, the comprehensive exposition of algorithms is introduced, encompassing not only the conventional CFAR detectors but also a specialized CFAR method tailored specifically to address the unique challenges posed by DSTs in section 4.2.

4.1. THE CARRADA DATASET

The Carrada dataset [29] is a public radar and camera dataset, recorded in Canada. The radar uses a Multiple Input Multiple Output (MIMO) system with 2 transmitter antennas (Tx) and 4 receiver antennas (Rx). Table 4.1 defines the capabilities and performance characteristics of the FMCW automotive radar system. **Carrier Frequency** is the operating frequency of the radar system, which is 77 GHz in this case. **Sweep Bandwidth** decides the range of frequencies covered during a single chirp, which is 4 GHz. This parameter determines the radar's range resolution. **Field of View** is the angular span of the radar's coverage, which is 180°, indicating the ability of this radar to scan objects within a given angular range. **Number of Chirps per Frame** describes the number of chirps sent during each frame, which is 64. **Number of Samples per Chirp** is the number of samples collected for each transmitted chirp, which is 256.

Parameter	Value
Carrier Frequency	77 GHz
Sweep Bandwidth	4 GHz
Maximum Range	50 m
Range Resolution	0.20 m
Maximum Radial Velocity	13.43 $m s^{-1}$
Radial Velocity Resolution	0.42 $m s^{-1}$
Field of View	180°
Number of Chirps per Frame	64
Number of Samples per Chirp	256

Table 4.1: Radar system parameters for the CARRADA dataset[29]

4.1.1. DATASET FEATURES AND DISTRIBUTION

The dataset documents range-Doppler in 2D matrices of size 256×64. The dataset consists of 30 sequences containing a total of 78 instances. The dataset spans 12,666 frames in total, with sequences having frame counts ranging from 157 to 1017, and an average of 422 frames per sequence [29]. Pedestrians, cyclists, and cars are recorded. To simulate urban driving scenarios, one or two objects are moving in the scene simultaneously and on different trajectories. The scenarios used in this thesis are simple with only a single target moving. The objects under detection are in motion, with movements ranging from approaching, receding, and moving from left to right or right to left. Figure 4.1 shows an example of a person moving away from the sensor. The distribution of these scenarios is depicted in Figure 4.2. Although the number of pedestrians is much higher than that of cyclists and vehicles, the unbiased distribution has no effect on the result because 300 frames are selected randomly from each object to guarantee an equal number.

Figure 4.1: A photo of a person moving away from the sensor for the sensor, as provided in the CARRADA dataset

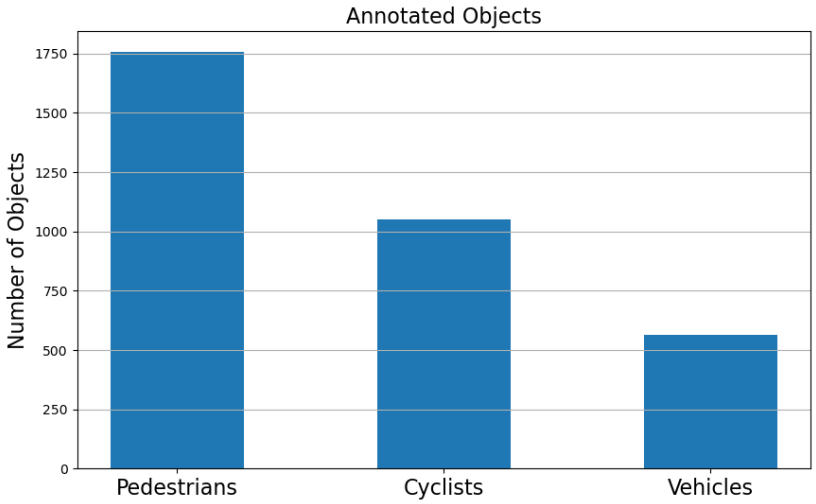

Figure 4.2: The distribution of three objects (pedestrians, cyclists, and vehicles) in the frames of the CARRADA dataset with only one single target.

Figure 4.3 shows the received radar signal following a series of essential pre-processing steps, displayed in RDM. Accompanied by the ground truth, this illustrates the target's accurate range and velocity information. The vertical blue line is the radar signal after the notch filter [30] which eliminates the disruptive effects of the clutter created by the ground reflections. Strong clutter reflections occasionally share comparable reflection intensities with target objects, thereby introducing unwanted incorrect signals into the estimation, which can interfere with accurate detection.

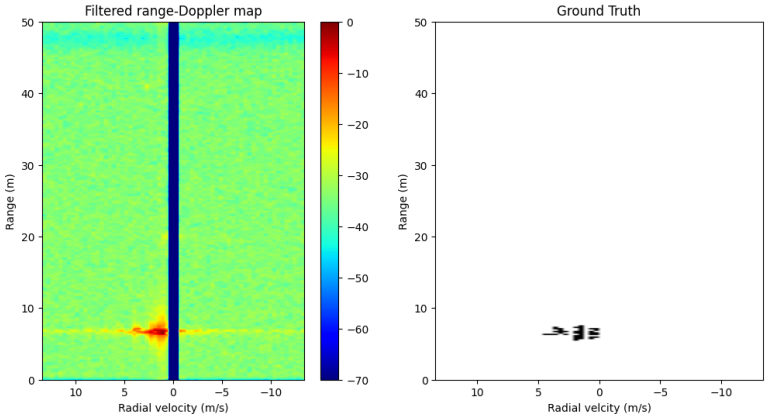

Figure 4.3: The received radar signal and the ground truth of a pedestrian 7m away from the sensor, moving towards the radar sensor.

4.1.2. PRE-PROCESSING

The signal processing chain is thoroughly explained in this section, with a visual representation provided in Figure 4.4.

1. RDM is generated by applying to 2D FFT, facilitating a clear visualization of the target's range and Doppler velocity but the clutter arising from ground reflections affects the original received radar signal.

2. Next, the pre-processing stage is executed, comprising two key elements: the application of a notch filter and amplitude normalization. The notch filter removes the influence of clutter arising from ground reflections [31]. Amplitude normalization is necessary to ensure consistency and comparability of signal strengths across different radar measurements and scenarios. By normalizing the amplitudes, radar signals from various sources can be standardized, facilitating accurate signal processing and subsequent analysis.

3. The final stage is target detection, a critical process achieved through a CFAR detector.

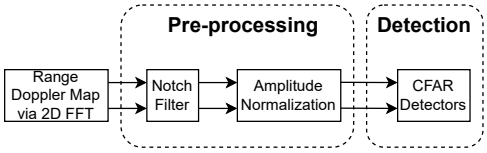

Figure 4.4: The signal processing chain implemented to process the CARRADA dataset, starting from RDM and ending at the radar target detection.

4.2. CONVENTIONAL CFAR ALGORITHMS

In this chapter, a detailed explanation of the two most widely used CFAR detectors and a special CFAR detector for DSTs is provided. When comparing it to 1D CFAR [23], the 2D CFAR approach considers both the range and Doppler dimensions during processing. In contrast, traditional methods focusing solely on either range or Doppler may not achieve the same level of effectiveness.

4.2.1. 2D CA-CFAR

Conventional 1D CA-CFAR estimates the clutter power by averaging the cells in the reference window and adjusting the detection threshold adaptively. However, it just estimates the potential target's Doppler or range position. To fully utilize the information in the RDM, 2D CFAR iterates all cells in the RDM and estimates the clutter power level. The design of the sliding reference window of 2D CA-CFAR is shown in Figure 4.5. Therefore, the potential target can be detected in the range and Doppler axes.

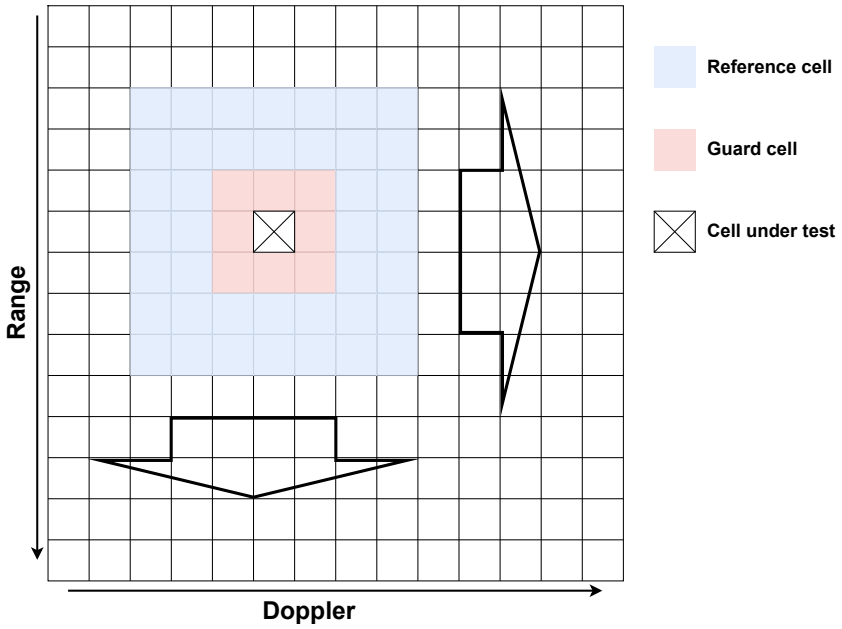

Figure 4.5: The design of sliding reference window of 2D CA-CFAR [12]. The CUT searches all units in RDM and estimates the arithmetic mean clutter in the reference window. The units in the guard window are ignored.

The estimated clutter power Z_{CA} is the arithmetic mean of cells in the two-dimensional reference window (4.1):

$$Z_{CA} = \frac{1}{N}\sum_{i=1}^{N} X_i \tag{4.1}$$

where N is the number of units inside the reference window. In Figure 4.5, the number of reference cells inside the blue area is 40. X_i is the i_{th} unit in the reference window.

The scaling factor T_{CA} of CA-CFAR [23] is determined by (4.2),

$$T_{CA} = N(p_{fa}^{-1/N} - 1) \tag{4.2}$$

Hence, the scaling factor is derived by employing fixed p_{fa} and a chosen reference window to estimate the clutter power. The detection threshold is decided by the product of the scaling factor and the estimated clutter power. In order to prevent outliers in the reference window, the guard window is set adjacent to the CUT, shown in the red area in Figure 4.5, because the units in the guard window are ignored and isolate the CUT from the reference window. Outliers refer to those radar echoes that significantly deviate from the expected statistical characteristics of the background clutter. Accordingly, implementing a guard window can be beneficial in enhancing stability. In this figure, there are 8 guard cells.

4.2.2. 2D OS-CFAR

2D OS-CFAR utilizes all samples in the reference window and ranks values in ascending order. The sequence is shown as (4.3):

$$X_{(1)} \leq X_{(2)} \leq X_{(3)} \leq ... \leq X_{(N-1)} \leq X_{(N)} \tag{4.3}$$

Then, the kth ordered value $X_{(k)}$ is selected to estimate clutter power. Generally, k is chosen between N/2 and 3N/4 [23]. Hence, the outliers in the reference window are difficult to hurt the estimation of clutter power level because the value of outliers is usually extremely large. After arranging elements in ascending order, outliers are on the two sides of the order, rather than in the middle. Therefore, the influence of outliers has been mitigated. For the same reason, the guard cells are unnecessary for OS-CFAR, which is demonstrated in Figure 4.6.

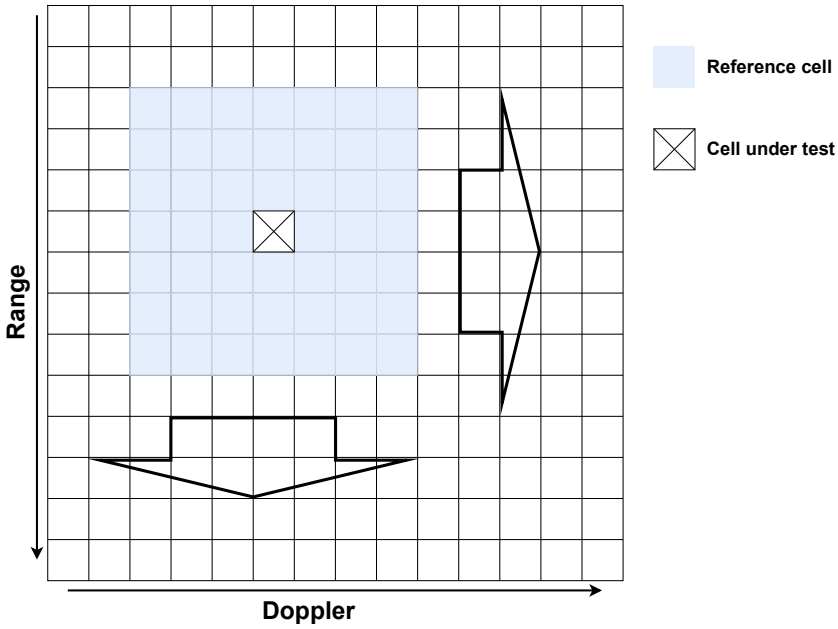

Figure 4.6: The design of sliding reference window of 2D OS-CFAR [12]. The CUT searches all units in RDM and chooses kth unit in the reference window based on a range of magnitude, in order to estimat the clutter power. There are no guard windows in 2D OS-CFAR because the outliers have no effect on the clutter power estimation.

The false alarm probability [23] has as follows (4.4):

$$p_{fa} = \frac{N!(T_{OS} + N - k)!}{(N-k)!(T_{OS} + N)!} \tag{4.4}$$

Accordingly, the scaling factor T_{OS} can be derived from (4.4) with fixed parameters of N, k and p_{fa}. However, the computation cost increases dramatically because the

iteration is from a 1D search in the range or Doppler bin to a 2D search in the range-Doppler and the search size becomes 2D, though the principle of 1D and 2D algorithm remains constant [32].

4.2.3. IMPROVED OS-CFAR

Pedestrians and cyclists are DSTs when limbs move forward and backward, leading to Doppler extension. There are multiple reflected radar points along the Doppler axis. In the range-Doppler plane, they manifest as horizontal lines that can be observed in Figure 4.7. Based on the characteristics of DSTs, W. Zhang et al. [17] introduce an OS-CFAR algorithm tailored to DSTs. The RCS of these VRUs is usually small, and the reflected energy is dispersed to multiple Doppler cells. Therefore, when the energy is gathered from multiple cells along the Doppler axis, it increases the capacity to detect potential targets.

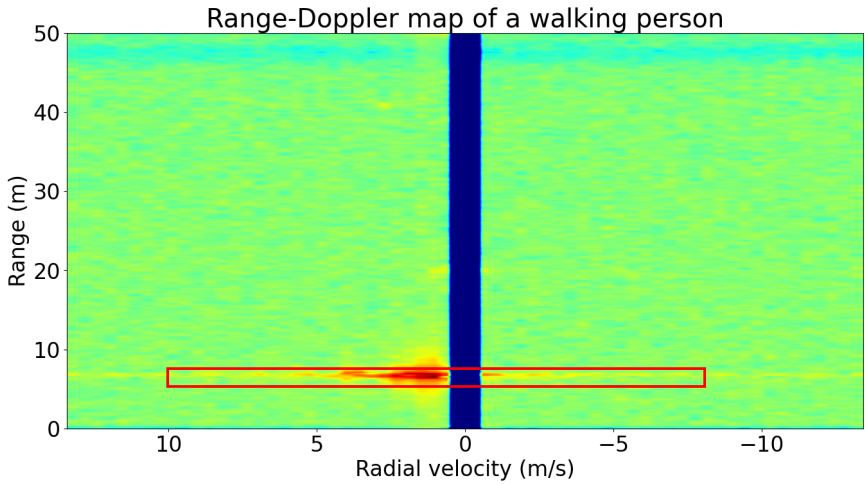

Figure 4.7: Example of RDM of a walking person as recorded in the CARRADA dataset

Algorithm 1 [17] introduces the improved OS-CFAR detection scheme tailored to DSTs. The dimension of RDM is $N \cdot M$, where N is the number of range bins and M is the number of Doppler bins. Denoted as $X_{n,l}$ in RDM, this element represents the target's range index (n) and Doppler frequency index (l). The variable D denotes the number of velocity resolution cells that the potential target occupies, with the nth range cell being the range under test. In this context, $2n_1$ corresponds to the number of reference range cells in this algorithm in Step 7.

The estimated clutter power Z is determined by the kth smallest reference unit in the reference window,

$$Z = Y_{(k)} \tag{4.5}$$

The p_{fa} is represented by [17]:

Algorithm 1 OS-CFAR tailored to DSTs [17]

1: **for** $n = 1, 2, \ldots, N$ **do**
2: **for** $l = 1, 2, \ldots, M - D + 1$ **do**
3: $Y_{n,l} = \sum_{d=0}^{D-1} \left| x_{n,l+d} \right|^2$
4: **end for**
5: Choose the maximum value Y_n in $(M - D + 1)$ summations
6: **end for**
7: Implement OS-CFAR in $[Y_{n-n_1}, \cdots, Y_{n-1}, Y_n, Y_{n+1}, \cdots Y_{n+n_1}]$
8: Repeat Step 7 to detect each range bin

$$
\begin{aligned}
p_{fa} = & m \begin{pmatrix} 2 \times n_1 \\ m \end{pmatrix} \int_0^{+\infty} \left(1 - \frac{\gamma(D, \alpha_{\mathrm{OS}} \cdot u)}{\Gamma(D)} \right) \\
& \times \left(1 - \frac{\gamma(D, u)}{\Gamma(D)} \right)^{2 \times n_1 - m} \left(\frac{\gamma(D, u)}{\Gamma(D)} \right)^{m-1} \\
& \times \frac{u^{(D-1)} e^{-u}}{\Gamma(D)} du
\end{aligned} \tag{4.6}
$$

where $\Gamma(z)$ is the gamma function and $\gamma(z, x)$ is the lower incomplete Gamma function, denoted as (4.7) and (4.8) respectively.

$$
\Gamma(z) = \int_0^{\infty} t^{z-1} e^{-t} dt \tag{4.7}
$$

$$
\gamma(z, x) = \int_0^{x} t^{z-1} e^{-t} dt \tag{4.8}
$$

4.2.4. SUMMARY

Unfortunately, a common challenge faced by conventional CFAR is the masking effect observed in multi-target and large-target scenarios. The masking effect occurs when the presence of multiple targets or large targets in the radar scene interferes with the accurate detection of individual targets, leading to worse performance [33]. The OS-CFAR procedure involves extensive computation, including sequence sorting and scaling factor calculations, which can be time-consuming [32]. Although the authors [17] propose a novel algorithm to enhance the detection performance of DSTs by utilizing the Doppler extension of pedestrians and cyclists, the Doppler position can not be detected because the cells along the Doppler axis have been accumulated and the information of Doppler position is lost. Therefore, an improved method is needed to find the Doppler velocity based on the introduced algorithm above.

4.3. PROPOSED OS-CFAR

After obtaining the potential range position of the target by the algorithm above, a further 1D OS-CFAR detector [23] is implemented in each detected line, shown in Figure 4.8.

The first picture is the original RDM under detection from the CARRADA dataset after pre-processing. Then, combining all detected lines after OS-CFAR tailored to DSTs [17] obtains the second figure. The range bins in the second figure are processed independently of each other. The detection of the Doppler position becomes feasible because of a further 1D OS-CFAR detector implemented. To provide further clarity and comprehension of the proposed algorithm, Figure 4.9 illustrates a real example of the detection process, capturing the movement of a walking person. The Range and Doppler position is clearly estimated in the third figure. For the robustness against outliers in multiple target scenarios, OS-CFAR is selected rather than CA-CFAR.

The probability of false alarm of 1D OS-CFAR and OS-CFAR tailored to DSTs is given as (4.4) and (4.6) respectively.

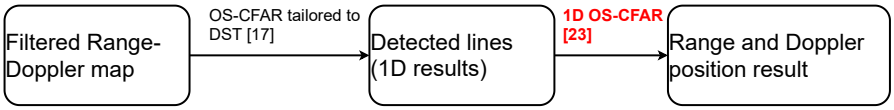

Figure 4.8: Proposed OS-CFAR schema

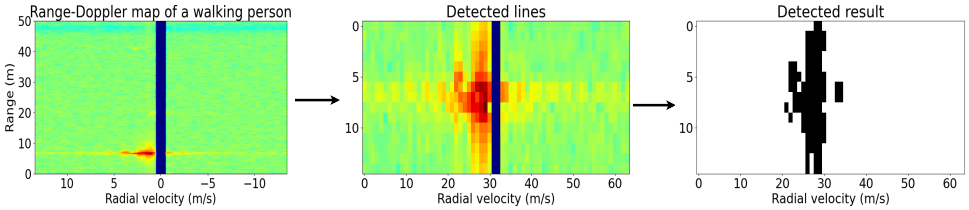

Figure 4.9: An example of the proposed OS-CFAR algorithm. The figure on the left shows the RDM after the notch filter [30]. The middle figure illustrates all detected lines. The figure on the right is the detection result.

4.4. SUMMARY

A detailed introduction of the utilized dataset has been provided in section 4.1, including the distribution of objects and the dataset's features. A signal processing chain starting from the collected radar data is explained and the processed range-Doppler matrix is detected by CFAR detectors. Having presented the 2D CA-CFAR, 2D OS-CFAR, OS-CFAR tailored to DSTs in section 4.2, a detection method is proposed to solve the failure to utilize the Doppler-spread information from pedestrians in section 4.3. The subsequent chapter will provide a comprehensive performance evaluation of these algorithms. This assessment aims to find out the strengths and limitations of these advanced radar detection techniques. The objective of the proposed method is to detect the radial velocity of the target to obtain more information about the target. The detection results will follow in the next chapter.

5

RESULTS

This chapter evaluates the performance of the introduced algorithms in radar target detection. Before performing the assessment, the ROC curve is introduced in section 5.1, a valuable tool for analyzing and comparing the algorithms' detection capabilities [34]. The ROC curve provides insights into the trade-off between p_d and p_{fa}. Following the ROC curve analysis, a parametric study is conducted to investigate the impact of various algorithm parameters on p_d and p_{fa} in section 5.2. The detection result of the study helps find out the optimal parameter settings for each algorithm. Additionally, different target objects are compared, including pedestrians, cyclists, and cars in section 5.3. Moreover, the computation time and complexity are analyzed between different detectors in section 5.4. Finally, the findings of this chapter are summarized, highlighting the strengths and limitations of the detectors in the real-world radar dataset.

5.1. ROC CURVE

To compare the detection performance of detectors in radar systems, a popular solution is to evaluate by the ROC curve, demonstrated as a plot of p_{fa} and p_d. The probability of detection p_d is defined by the pixels of ground truth detected by the detector N_d over the total number of the pixels of ground truth N_{gt}, shown as (5.1).

$$p_d = \frac{N_d}{N_{gt}} \tag{5.1}$$

ROC curves are acquired using 300 frames of each target in the performance analysis in this thesis. With fixed p_{fa} from 10^{-6} to 10^{0}, ROC curves are derived.

To provide a clear explanation of ROC curve, a sample plot of ROC curve is demonstrated in Figure 5.1. In ROC curve, each point on the curve represents a specific detection performance.

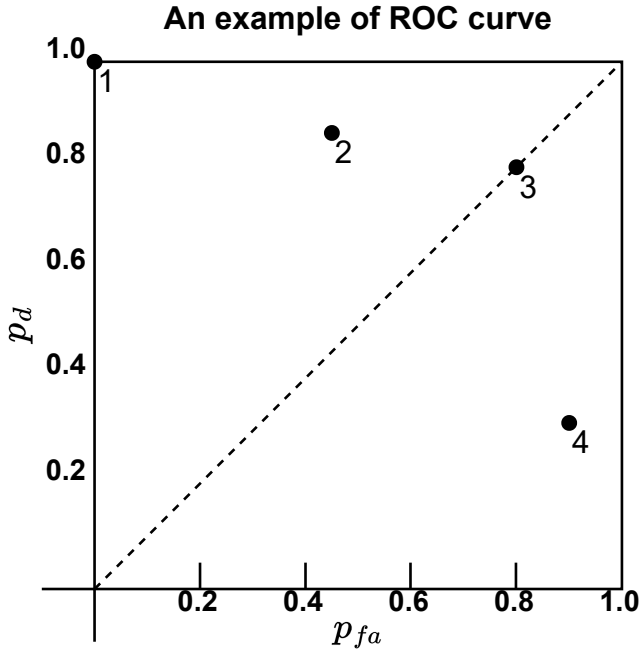

Figure 5.1: A plot of ROC curve, including four detection performances shown as the black point. A perfect detector works at the (0,1) point, representing no false alarms and 100% detected points in the ground truth. Points above the dashed line denote good detection performance, exceeding the random performance, such as point 2. A random detector will have a curve that lies along the diagonal line from the bottom left to the top right, representing an equal chance of true positives and false positives. Points below the diagonal line denote unsatisfactory results, performing worse than random.

5.2. PARAMETRIC STUDY OF DIFFERENT CFAR DETECTORS

Before presenting the results of the ROC curve analysis, the parametric study of CA-CFAR and OS-CFAR detectors investigates the influence of various parameters on their detection performance. Through a systematic analysis, key parameters such as the number of guard cells and the number of reference cells are varied to observe their impact on the ROC curve. After the parametric study, optimal parameter settings strike a balance between more accurate target detection and economic computation cost, because the 2D searching in RDM spends more running time compared to 1D searching and the detection performances are analyzed with 300 frames.

With the fixed number of guard cells, the computation complexity increases with the size of the reference window. Therefore, only two sets of reference cells are tested. Figure 5.2 provides a visual depiction of the key variables that influence the performance of CA-CFAR in target detection. These essential parameters include the number of guard cells in the range bin, the number of guard cells in the Doppler bin, the number of refer-

ence cells in the range bin, and the number of reference cells in the Doppler bin.

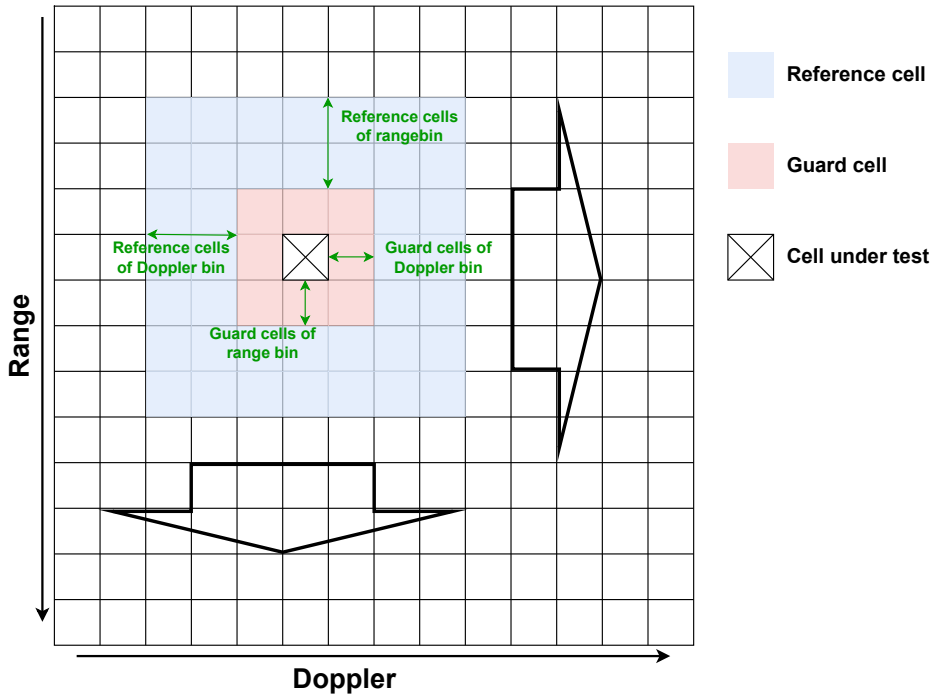

Figure 5.2: The figure of explanation of the number of guard cells and the number of reference cells

Table 5.1 presents the parameter settings for the parametric study conducted on CA-CFAR and OS-CFAR detectors. The three different parameter configurations of CA-CFAR are abbreviated as ca1, ca2, and ca3. For OS-CFAR, the abbreviations are os1 and os2. The reason why the guard cells are missing in OS-CFAR is that the influence of outliers is limited for OS-CFAR which has been explained in the previous chapter.

	N_{GR}	N_{GD}	N_{TR}	N_{TD}
ca1	2	2	4	4
ca2	2	2	8	8
ca3	4	4	8	8
os1	-	-	4	4
os2	-	-	8	8

Table 5.1: Parameter settings. In CA-CFAR, three different parameter sets, namely ca1, ca2, and ca3, are examined, with varying numbers of guard and reference cells for range and Doppler bins. For OS-CFAR, two parameter sets of os1 and os2 are investigated.

where,

- N_{GR} is the number of the guard cells of range bins
- N_{GD} is the number of the guard cells of Doppler bins
- N_{TR} is the number of the training cells of range bins
- N_{TD} is the number of the training cells of Doppler bins

Specifically, ca1 uses 2 guard cells in range and Doppler bin and 4 reference cells in range and Doppler bin, ca2 employs 2 guard cells in range and Doppler bin and 8 reference cells in range and Doppler bin, while ca3 implements 4 guard cells in range and Doppler bin and 8 reference cells in range and Doppler bin. In this case, only the reference cells for range and Doppler bins are considered, with 4 reference cells for os1 and 8 reference cells for os2. ROC curves for both algorithms are shown in Figure 5.3 providing a comprehensive assessment of different targets' detection performances across various parameter settings.

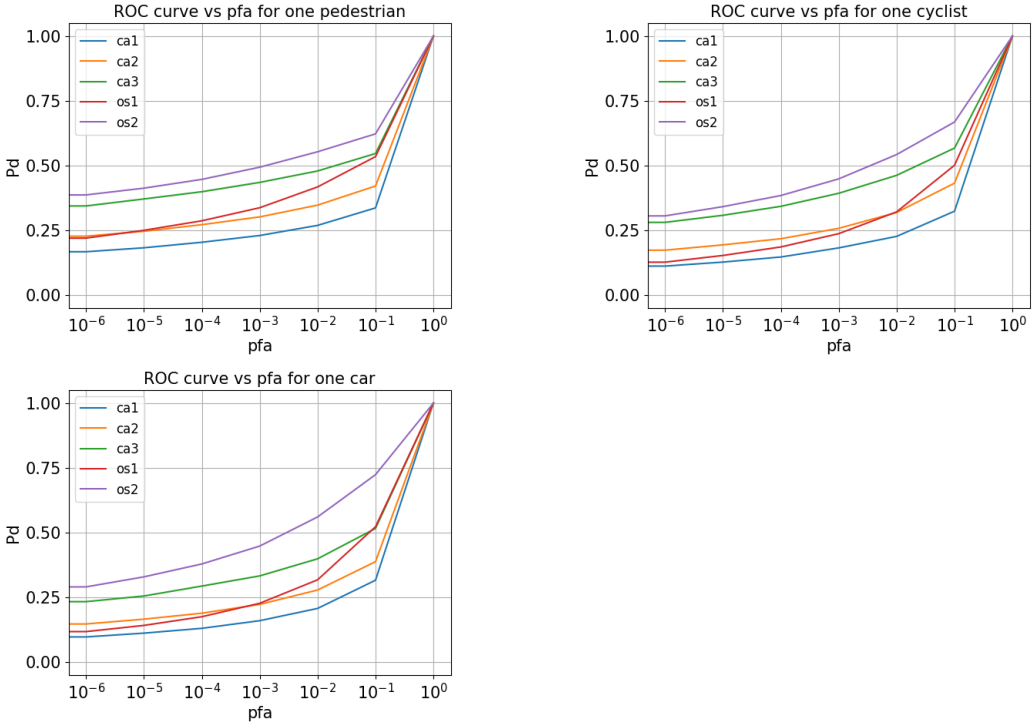

Figure 5.3: ROC curve of one pedestrian, one cyclist and one car. Comparison of conventional CA-CFAR and OS-CFAR algorithms with different parameter settings.

The investigation of CA-CFAR's performance is interesting when employing a larger guard window (4 cells in both range and Doppler bins, green curve) while maintaining

a constant reference window size. p_d with the parameter setting of ca2 (orange curve) is lower than that of ca3. The larger guard window includes more background clutter, leading to increased background interference during target detection, affecting the algorithm's false alarm rate. The range resolution of this radar system is 0.2m [29] so that the target with large size, such as cars, cyclists, and pedestrians, will occupy multiple range and Doppler cells in RDM. If increasing the size of the guard window, though more units will be taken into consideration, it will also isolate the reflected signal in RDM. For the same reason, the detection performance of pedestrians is better than that of the other two objects under the same parameter setting of the same CFAR detector.

Compared to CA-CFAR, OS-CFAR witnesses superior performance under the condition of the same reference window size (purple curve and orange curve, red curve and blue curve). OS-CFAR is more robust to variations in clutter intensity and is capable of effectively eliminating clutter fluctuations resulting in a lower p_{fa} and a higher p_d. On the other hand, CA-CFAR detector relies on averaging the power levels of the reference cells in the window to estimate the background clutter. Although this method can provide an accurate estimation of the clutter level in homogeneous clutter environments, it might encounter challenges in scenarios with non-homogeneous clutter or strong interference from multiple objects. Consequently, CA-CFAR may be more susceptible to false alarms and might exhibit reduced p_d in detecting weak targets compared to OS-CFAR.

5.3. PERFORMANCE COMPARISON

After conducting the parametric study and identifying the optimal parameter settings, the optimal parameter setting of CA-CFAR and OS-CFAR is selected, which are ca3 and os2. Although an improved OS-CFAR tailored to DSTs was introduced in the previous chapter, this algorithm is not involved in the comparison because it only detects the range position, showing a 1D result. Therefore, compared to 2D CA-CFAR and OS-CFAR, the detection performance cannot be analyzed equally. However, the result of the proposed CFAR method introduced in section 4.3 is a 2D result of range and Doppler position. In Figure 5.4, ROC curves are demonstrated with fixed p_{fa} from 10^{-6} to 10^{0} by comparing the three algorithms with three objects comprehensively. Meanwhile, a random detector is shown as a dashed line, indicating an equivalent likelihood of true positives and false positives.

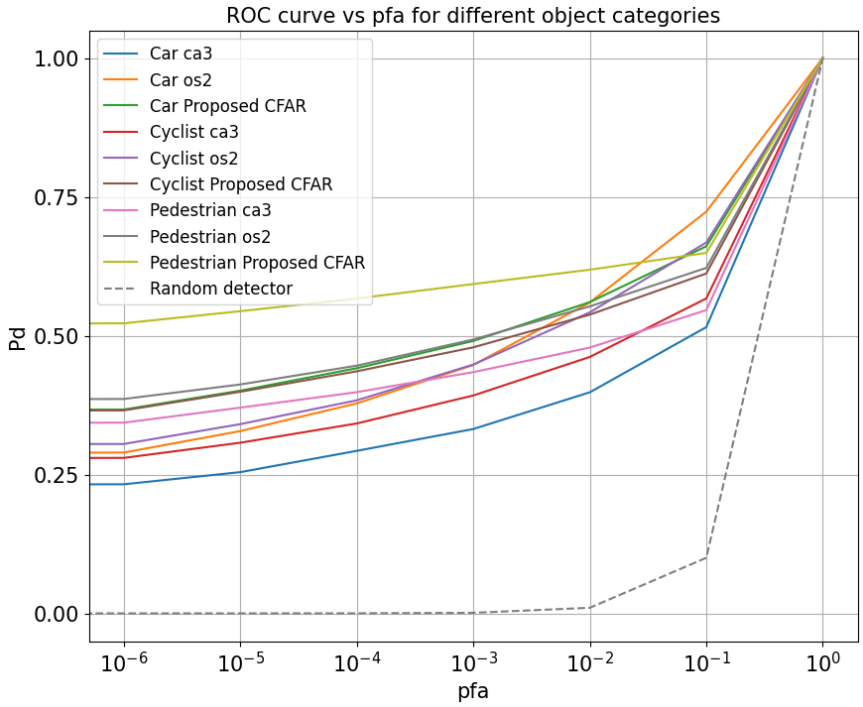

Figure 5.4: The performance of selected CFAR detectors on different object categories.

As expected, the proposed CFAR detector exhibits better performance in scenarios with DSTs, outperforming both CA-CFAR and OS-CFAR, especially the curve of one pedestrian using the proposed CFAR method. With p_{fa} under 10^{-2}, the detection performance of the proposed CFAR detector exceeds that of CA-CFAR and OS-CFAR when detecting the same type object, because the proposed CFAR algorithm is specifically tailored to address the challenges posed by DSTs, which spread the reflected energy to multiple Doppler bins. Additionally, a car, as a large size and strong reflection target, should be more detectable compared to pedestrians and cyclists with low RCS. However, its p_d is always lower than that of pedestrians and cyclists when using CA-CFAR and OS-CFAR detectors. It probably results from the size of the window of CA-CFAR and OS-CFAR does not fit the size of the car in RDM. Therefore, more parameter sets can be attempted, but due to limitations in computational capacity and time, this aspect can only be considered as a part of future work.

To provide a clearer visualization, the optimal parameter setting of conventional 2D CA-CFAR and 2D OS-CFAR are compared to the proposed CFAR detector and the random detector of each object (pedestrian, cyclist and car) in Figure 5.5. It is shown that p_d of the proposed CFAR detector (the green line in each subfigure) outperforms CA-CFAR and OS-CFAR for each target with p_{fa} under 10^{-2}. Also, there is a large improvement when detecting a pedestrian, especially with low p_{fa}.

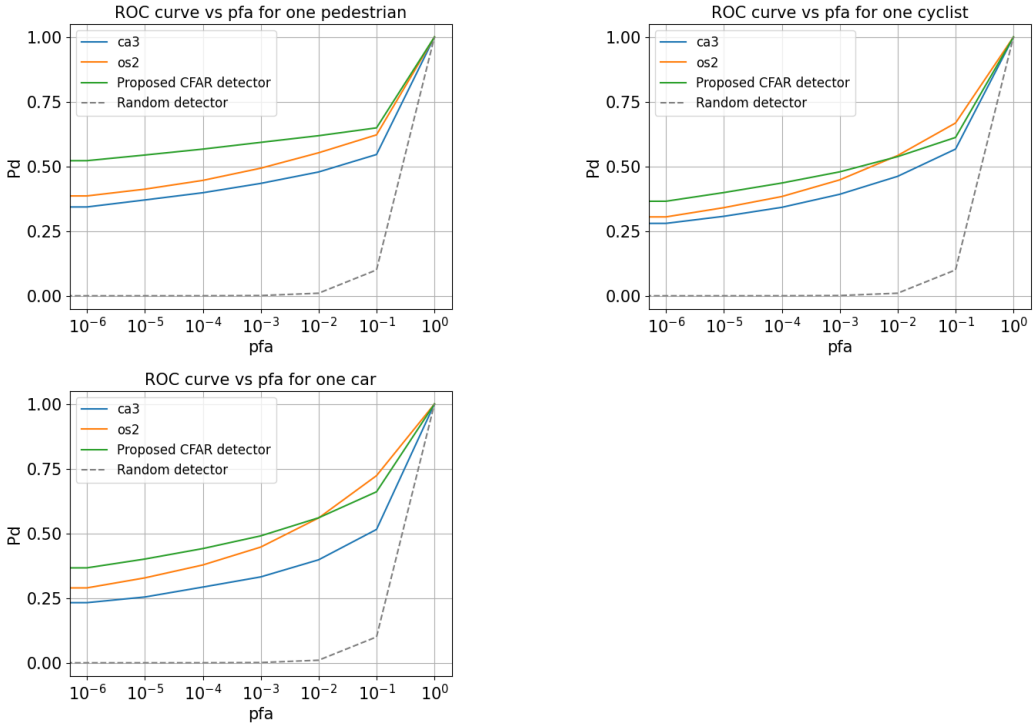

Figure 5.5: ROC curve of one pedestrian, one cyclist and one car. Comparison of the optimal parameter setting of conventional 2D CA-CFAR and 2D OS-CFAR algorithms with the the proposed CFAR detector and random detector.

5.4. COMPUTATIONAL COST

Table 5.2 summarizes the computation cost of three objects by using 300 frames for each object. With the increase in the size of the guard window and reference window, the algorithm spends more time in searching and computation in CA-CFAR and OS-CFAR. The proposed CFAR method not only shows a higher p_d with the same p_{fa}, but also it saves more running time because it filters out many uninterested range bins and then implements 1D searching along Doppler axis. Whereas, 2D CA-CFAR and 2D OS-CFAR will go through all units in RDM, leading to much more computation time.

CFAR detectors	Pedestrian	Cars	Cyclists
ca1	176s	170s	173s
ca2	400s	515s	408s
ca3	889s	983s	867s
os1	557s	539s	547s
os2	1264s	1141s	1293s
Proposed CFAR detector	69s	77s	74s

Table 5.2: The computation time of CFAR detectors under different parameter settings in seconds. Conventional CA-CFAR and OS-CFAR are compared with different parameter settings, as well as the proposed detector.

5.5. SUMMARY

To study the detection performance of different CFAR detectors, ROC is introduced and then used to analyze the performance of aforementioned algorithms in chapter 4. In conclusion, the proposed OS-CFAR outperformance than 2D CA-CFAR and 2D OS-CFAR with the same p_{fa}.

Before presenting the results of the ROC curves, the parametric study of CA-CFAR and OS-CFAR detectors is conducted to investigate the influence of various parameters on their detection performance. Although increasing the size of the guard window and reference window holds the potential to enhance the detection capabilities, for the sake of economic computation costs three parameter sets of CA-CFAR and two sets of OS-CFAR are selected. It is very important to choose an appropriate size of the guard and reference window to balance the sensitivity of detecting targets and accurately estimate the clutter power.

The choice of window size will differ for targets with different sizes. Based on the idea of OS-CFAR tailored to DSTs [17], the proposed method aims to provide an accurate detection result of range and Doppler positions, which also shows more accurate detection results with p_{fa} under 10^{-2} than 2D CA-CFAR and 2D OS-CFAR. It accumulates the dispersed energy of DSTs to make a stronger reflected echo energy and implements 1D OS-CFAR. The extension of DSTs such as pedestrians and cyclists in radar primarily occurs within the Doppler bins. The detection performance of DSTs witnessed an improvement when using the proposed CFAR. Despite having a larger size and RCS, cars exhibited a lower p_d in ca3 and os2 in Figure 5.4 compared to pedestrians and cyclists. This outcome might result from the size of the windows is not large enough. Ideally, a larger window size will help improve the detection performance while the computation time will increase heavily. For the sake of limited time, larger window sizes are not considered in this thesis.

More importantly, the proposed algorithm witnessed a dramatic drop in running time because it finds the potential range bins first and then implements 1D searching along the Doppler axis, while if it is employed in a multi-target scenario, the computation time is expected to increase.

6

CONCLUSIONS

This chapter summarizes the results and the contributions of the thesis. Moreover, it offers recommendations for potential avenues of future research.

6.1. CONCLUSIONS

The thesis explores the detection performance with three types of targets with pedestrians, cyclists and vehicles by applying different CFAR detectors. At first, the sensors on AVs which are directly related to the detection performance of surroundings play a vital role in realizing "Full driving autonomy" (Level 5). After comparing the pros and cons of different sensors, the abilities of FMCW radar to provide accurate range and velocity measurement of objects in relation to the radar and robustness of all-weather conditions make FMCW radar an essential sensor in AVs systems. During the literature review, two main research gaps are pointed out:

1. **Scarce validation on public real-world radar dataset.** The assessment of detectors via the publicly available real-world traffic datasets holds significant significance. Real-world datasets include practical environmental information and vehicular actions that may not be fully replicated in simulated settings. Furthermore, the adoption of a public real-world dataset contributes to the comparability of various radar detectors within the same scenario.

2. **Conventional CFAR detectors are typically not designed for DSTs but many VRUs are extended targets, such as pedestrians.** CA-CFAR and OS-CFAR are two conventional detectors that fail to utilize the Doppler-spread information from pedestrians.

The enhancement of detection outcomes is visualized through the utilization of two types of charts, ROC curves of selected CFAR detectors on different object categories and the computation time of three CFAR detectors under different parameter settings in seconds. The proposed CFAR detector demonstrates better performance in scenarios involving DSTs, outperforming both CA-CFAR and OS-CFAR, particularly evident in the

performance curve of the proposed CA-CFAR for pedestrian detection. The proposed algorithm exhibits a significant reduction in running time as it identifies potential range bins first, followed by 1D searching along the Doppler axis. In contrast, 2D CA-CFAR and 2D OS-CFAR require scanning through all units in RDM, resulting in longer computation time.

6.2. RECOMMENDATIONS

This section aims to suggest some work to be done in the future. Suggestions are given as follows:

- The distribution of CARRADA dataset is followed by Weibull distribution, demonstrated in Appendix 6.2. CFAR detectors based on the statistical properties of the received signals. Understanding the clutter distribution enables the detector to determine the appropriate statistical metric, such as median or mean, for setting the detection threshold. This ensures that the detector maintains a consistent false alarm rate while effectively detecting targets. Therefore, potential improvements can be realized by studying the parameter estimation of target clutter.
- Due to limitations in computational capacity and time, more parameter sets are not done to explore the influence of larger window sizes on large-size targets. Therefore, more ROC analysis can be studied by increasing the number of reference and guard windows. In addition, more frames of targets can also be investigated.

BIBLIOGRAPHY

[1] Iis P Tussyadiah, Florian J Zach, and Jianxi Wang. "Attitudes toward autonomous on demand mobility system: The case of self-driving taxi". In: *Information and Communication Technologies in Tourism 2017: Proceedings of the International Conference in Rome, Italy, January 24-26, 2017*. Springer. 2017, pp. 755–766.

[2] D Mohr, D Wee, and T Möller. "Eight disruptive trends shaping the auto industry of 2030". In: *Autom. Megatrends Mag.* 1 (2016), pp. 8–10.

[3] Thomas A Hemphill. "Autonomous vehicles: US regulatory policy challenges". In: *Technology in Society* 61 (2020), p. 101232.

[4] World Health Organization et al. "Global status report on road safety 2018: Summary". In: *World Health Organization* (2018).

[5] Santokh Singh. *Critical reasons for crashes investigated in the national motor vehicle crash causation survey*. Tech. rep. 2015.

[6] Claire Pilet, Céline Vernet, and Jean-Louis Martin. "Estimated crash avoidance with the hypothetical introduction of automated vehicles: a simulation based on experts' assessment from French in-depth data". In: *European transport research review* 13 (2021), pp. 1–8.

[7] Daniel J Fagnant and Kara Kockelman. "Preparing a nation for autonomous vehicles: opportunities, barriers and policy recommendations". In: *Transportation Research Part A: Policy and Practice* 77 (2015), pp. 167–181.

[8] Sae International. "Taxonomy and definitions for terms related to driving automation systems for on-road motor vehicles". In: *SAE international* 4970.724 (2018), pp. 1–5.

[9] *National Highway Traffic Safety Administration, Automated vehicles for safety*. https://www.nhtsa.gov/technology-innovation/automated-vehicles-safety.

[10] Zhangjing Wang, Yu Wu, and Qingqing Niu. "Multi-Sensor Fusion in Automated Driving: A Survey". In: *IEEE Access* 8 (2020), pp. 2847–2868. DOI: 10.1109/ACCESS.2019.2962554.

[11] Arthur Venon et al. "Millimeter Wave FMCW RADARs for Perception, Recognition and Localization in Automotive Applications: A Survey". In: *IEEE Transactions on Intelligent Vehicles* 7.3 (2022), pp. 533–555. DOI: 10.1109/TIV.2022.3167733.

[12] Matthias Kronauge and Hermann Rohling. "Fast Two-Dimensional CFAR Procedure". In: *IEEE Transactions on Aerospace and Electronic Systems* 49.3 (2013), pp. 1817–1823. DOI: 10.1109/TAES.2013.6558022.

[13] Yishan Ye et al. "Doppler-Spread Targets Detection for FMCW Radar Using Concurrent RDMs". In: *IEEE Transactions on Vehicular Technology* 71.11 (2022), pp. 11454–11464. DOI: 10.1109/TVT.2022.3190478.

[14] Youngwook Kim et al. “Human Detection Based on Time-Varying Signature on Range-Doppler Diagram Using Deep Neural Networks”. In: *IEEE Geoscience and Remote Sensing Letters* 18.3 (2021), pp. 426–430. DOI: 10.1109/LGRS.2020.2980320.

[15] Karsten Thurn et al. “Pedestrian detection with an interlaced chirp sequence concept in automotive radar”. In: *2015 16th International Radar Symposium (IRS)*. 2015, pp. 161–166. DOI: 10.1109/IRS.2015.7226344.

[16] Eugin Hyun, Young-Seok Jin, and Jong-Hun Lee. “A pedestrian detection scheme using a coherent phase difference method based on 2D range-Doppler FMCW radar”. In: *Sensors* 16.1 (2016), p. 124.

[17] Wei Zhang et al. “Enhanced Detection of Doppler-Spread Targets for FMCW Radar”. In: *IEEE Transactions on Aerospace and Electronic Systems* 55.4 (2019), pp. 2066–2078. DOI: 10.1109/TAES.2019.2925433.

[18] N. Yamada, Y. Tanaka, and K. Nishikawa. “Radar cross section for pedestrian in 76GHz band”. In: *2005 European Microwave Conference*. Vol. 2. 2005, 4 pp.–1018. DOI: 10.1109/EUMC.2005.1610101.

[19] Domenic Belgiovane et al. “77 GHz radar scattering properties of pedestrians”. In: *2014 IEEE Radar Conference*. 2014, pp. 0735–0738. DOI: 10.1109/RADAR.2014.6875687.

[20] Deborah J Rumsey. *Statistics for dummies*. John Wiley & Sons, 2016.

[21] D.A. Abraham. “Chapter 11 - Signal Processing”. In: *Applied Underwater Acoustics*. Ed. by Thomas H. Neighbors and David Bradley. Elsevier, 2017, pp. 743–807. ISBN: 978-0-12-811240-3. DOI: https://doi.org/10.1016/B978-0-12-811240-3.00011-4. URL: https://www.sciencedirect.com/science/article/pii/B9780128112403000114.

[22] Mohamed Baadeche, Faouzi Soltani, and Fulvio Gini. “Performance comparison of mean-level CFAR detectors in homogeneous and non-homogeneous Weibull clutter for MIMO radars”. In: *Signal, Image and Video Processing* 13 (2019), pp. 1677–1684.

[23] Hermann Rohling. “Radar CFAR Thresholding in Clutter and Multiple Target Situations”. In: *IEEE Transactions on Aerospace and Electronic Systems* AES-19.4 (1983), pp. 608–621. DOI: 10.1109/TAES.1983.309350.

[24] V. Gregers Hansen and James H. Sawyers. “Detectability Loss Due to "Greatest Of" Selection in a Cell-Averaging CFAR”. In: *IEEE Transactions on Aerospace and Electronic Systems* AES-16.1 (1980), pp. 115–118. DOI: 10.1109/TAES.1980.308885.

[25] G.V. Trunk. “Range Resolution of Targets Using Automatic Detectors”. In: *IEEE Transactions on Aerospace and Electronic Systems* AES-14.5 (1978), pp. 750–755. DOI: 10.1109/TAES.1978.308625.

[26] Harold M Finn. “Adaptive detection mode with threshold control as a function of spatially sampled clutter-level estimates”. In: *Rca Rev.* 29 (1968), pp. 414–465.

[27] Ahsan Jalil, Hassan Yousaf, and Muhammad Iram Baig. "Analysis of CFAR techniques". In: *2016 13th International Bhurban Conference on Applied Sciences and Technology (IBCAST)*. IEEE. 2016, pp. 654–659.

[28] H. Rohling and R. Mende. "OS CFAR performance in a 77 GHz radar sensor for car application". In: *Proceedings of International Radar Conference*. 1996, pp. 109–114. DOI: 10.1109/ICR.1996.573784.

[29] Arthur Ouaknine et al. "Carrada dataset: Camera and automotive radar with range-angle-doppler annotations". In: *2020 25th International Conference on Pattern Recognition (ICPR)*. IEEE. 2021, pp. 5068–5075.

[30] B.-E. Tullsson. "Topics in FMCW radar disturbance suppression". In: *Radar 97 (Conf. Publ. No. 449)*. 1997, pp. 1–5. DOI: 10.1049/cp:19971620.

[31] Mi He et al. "Polarimetric extraction technique of atmospheric targets based on double sLdr and morphology". In: *2011 IEEE International Geoscience and Remote Sensing Symposium*. 2011, pp. 3245–3248. DOI: 10.1109/IGARSS.2011.6049911.

[32] H. Rohling and R. Mende. "OS CFAR performance in a 77 GHz radar sensor for car application". In: *Proceedings of International Radar Conference*. 1996, pp. 109–114. DOI: 10.1109/ICR.1996.573784.

[33] Chunmei Xu et al. "An improved CFAR algorithm for target detection". In: *2017 International Symposium on Intelligent Signal Processing and Communication Systems (ISPACS)*. 2017, pp. 883–888. DOI: 10.1109/ISPACS.2017.8266600.

[34] Tom Fawcett. "An introduction to ROC analysis". In: *Pattern Recognition Letters* 27.8 (2006). ROC Analysis in Pattern Recognition, pp. 861–874. ISSN: 0167-8655. DOI: https://doi.org/10.1016/j.patrec.2005.10.010. URL: https://www.sciencedirect.com/science/article/pii/S016786550500303X.

[35] Qiangwen Zheng et al. "A Target Detection Scheme With Decreased Complexity and Enhanced Performance for Range-Doppler FMCW Radar". In: *IEEE Transactions on Instrumentation and Measurement* 70 (2021), pp. 1–13. DOI: 10.1109/TIM.2020.3027407.

[36] Yunhan Dong. *Distribution of X-band high resolution and high grazing angle sea clutter*. Citeseer, 2006.

APPENDIX

This appendix demonstrates the fitting of a Weibull distribution to the experimental data used in this thesis. This could be used in future work for a better estimation of the detection threshold.

The road clutter shows similarities to Weibull clutter [35]. The Weibull distribution is a two-parameter distribution and the probability density function (PDF) [36] can be expressed as (1),

$$f(x;k,b) = bkx^{k-1}e^{-bx^k} \tag{1}$$

where k is the shape parameter and b is the scale parameter. The Weibull distribution serves the exponential distribution (k=1) and the Rayleigh distribution (k=2).

The cumulative distribution function (CDF) is determined by (2),

$$F(x;k,b) = 1 - e^{-bx^k} \tag{2}$$

Figure 1 shows the distribution of the clutter data (blue) and the curve of the Weibull distribution (red). All non-target units are sampled and demonstrated in the bar chart. The PDF result provides clear evidence that the clutter power is well-fitted by the Weibull distribution. Therefore, more improvement could be around the distribution of the clutter power to enhance the probability of detection.

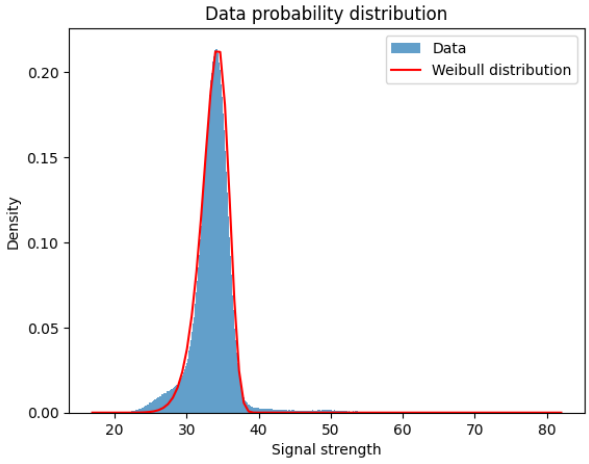

Figure 1: The PDF of Carrada dataset and the Weibull distribution. The fitting result indicates a close match between the PDF of clutter power and the Weibull distribution.